Special nuclear material detection with a mobile multi-detector system

D. Cester[1] , G. Nebbia[2], L. Stevanato [1,2] ,G. Viesti[1,2,*], F. Neri[3] , S. Petrucci[3] , S. Selmi[3] ,C. Tintori[3], P. Peerani[4] , A. Tomanin[4]

[1] *Dipartimento di Fisica, Università di Padova, Via Marzolo 8, I-3513 Padova 1, Italy*
[2]*INFN Sezione di Padova, Via Marzolo 8, I-35131 Padova , Italy*
[3]*CAEN S.p.A., Via Vetraia 11, I-55049, Viareggio (LU), Italy*
[4] *European Commission EC–JRC–ITU, I-21027 Ispra, Italy*

Abstract.

The detection of special nuclear material has been studied with a mobile inspection system used both as a high sensitivity passive neutron/gamma spectroscopic tool and as an active inspection device using tagged neutrons. The detection of plutonium samples seems to be possible with passive interrogation, even for small samples, thanks to the yield of gamma ray and neutrons. Moreover the gamma ray spectrum shows clear signatures related to ^{239}Pu. The passive detection of uranium is much more difficult because of the low neutron yield and of the easiness of shielding the gamma ray yield of highly enriched U samples. However, we show that active interrogation with tagged neutrons is able to provide signatures for the discrimination of uranium against other heavy metals.

Pacs: 29.40.-n, 27.90.+b, 28.20.-v , 89.20.Bb

Keywords: Special Nuclear Material, mobile detection system, digital signal processing, neutron and gamma ray measurements, neutron induced reactions.

*Corresponding author: Tel/Fax: +39 8275933, viesti@pd.infn.it

Submitted to Nuclear Instruments and Method A

1. INTRODUCTION

The SLIMPORT project [1], financed by the Italian Ministry for the Economic Development (MISE), is dedicated to the development of an integrated toolbox forming a complete security system to monitor the flow of persons and merchandise in harbours. In this framework, a mobile inspection station (called SMANDRA, the Italian acronym stands for Sistema Mobile per Analisi Non Distruttive e RAdiometriche) has been developed. The system is conceived as an instrument to perform non-destructive analysis, usable in conjunction with present monitoring devices such as radiation portal monitors, x-ray scanners and others. The aim of the system is to detect and identify sources of ionizing radiation or dangerous and/or illegal materials inside volumes tagged as "suspect" by conventional X-ray scanners. The system is made of two parts :

1. A passive unit including gamma-ray and neutron detectors. The unit hosts batteries, power supplies, front-end electronics and CPU.
2. An active unit including a portable sealed neutron generator used to produce tagged neutron beams.

The first unit can be used in standalone mode as a high efficiency spectroscopic radiometer for the detection and identification of ionizing radiation such as gamma-rays, fast and thermal neutrons produced by radioactive sources or Special Nuclear Material (SNM). It can be used as well as detector package connected to the second unit for active interrogation of voxels inside a load using the Tagged Neutron Inspection System (TNIS) technique [2].

The application of the SMANDRA multi-detector system to the detection of SNM is described in this paper. Laboratory results are reported for passive as well as for active interrogations of SNM.

2. THE SMANDRA SYSTEM

A complete description of the SMANDRA system is presented in [3], here we report only the relevant parameters of the system. The dual use of SMANDRA (active and passive interrogations) sets stringent requirements: a) low background, high efficiency detectors for gamma and neutrons, b) capability of discriminating the two components of the radiation in the passive mode and c) high count rate capability to operate in coincidence with the associated particle counter hosted in the neutron generator.

Photon spectroscopy is performed using a high resolution 2" x 2" BrilLanCe^{TM} 380 LaBr(Ce) detector and a high efficiency large volume 5" x 5" NaI(Tl) scintillator. The LaBr(Ce) detector offers the ultimate energy resolution for scintillators but suffers from internal activity [4], thus showing some limitations in the detection and identification of weak ^{40}K sources [5]. Moreover, these crystals are presently available only with modest volumes compared to other scintillators, therefore this entails limitations in the active mode operation when energetic gamma rays of up to 6 MeV from inelastic excitation of oxygen and carbon nuclei need to be detected [6]. A large NaI(Tl) scintillator has been therefore selected to be used as the primary detector for energetic gamma rays in active investigations as well as high efficiency device in the detection and identification of weak gamma sources. The gamma ray detectors were operated in passive mode measurements with very low energy thresholds. In particular the NaI(Tl) detector could clearly identify the 59 keV ^{241}Am gamma line.

A ^{3}He proportional counter with a polyethylene moderator is a typical choice as neutron counter for systems operated in passive mode [7]. However, direct detection of fast neutrons both in passive and active mode is an important plus, as shown below, and imposes the use of a liquid organic scintillator. The interest in the detection of fast neutrons is motivated by the 1/E energy dependence of the cosmic-ray induced neutron background making the differential flux at about 1

MeV six orders of magnitude lower compared to 1 eV [8]. Consequently, the signal-to-noise ratio obtained selecting fast neutrons should be more effective in detecting weak, un-moderated sources. In the SMANDRA system a 5" x 2" NE213 and an ASPECT SN-01 ^{3}He proportional counter were employed as neutron detectors. The liquid scintillator was operated at very low threshold. However, the acceptance of a neutron event was obtained by energy windowing between 400 keVee and 1700 keVee, which corresponds to about 1.7-7.4 MeV neutron energy, in order to avoid gamma-ray contamination at low pulse height and optimize the signal-to-noise ratio with respect to the neutron natural background.

An important distinctive factor of the SMANDRA system is that both operating modes (passive and active) are managed by a simple CAEN VME electronic front end based on fast digitizers. The front end makes use of a prototype battery operated VME mini-crate (4 slots) with a Bridge USB V1718. The mini-crate hosts a HV system (V6533 Programmable HV Power Supply (6 Ch., 4 kV, 3 mA, 9 W) and a V1720 8 Channel 12bit 250 MS/s Digitizer. Inside the V1720, Digital Pulse Processing (DPP) algorithms are implemented by using FPGA, providing on-line for each event a) a time stamp, b) a complete integration of the signal, c) a partial integration of the signal used for Pulse Shape Discrimination (PSD) in the liquid scintillator and d) the possibility of storing a selected part of the digitized signal. The last feature is needed in order to reconstruct off-line coincidences and time-of-flight spectra in active mode.

The results reported in this paper have been obtained by using calibration gamma ray-sources and neutron sources (^{252}Cf and AmBe) in our Applied Physics Laboratory located inside the INFN-LNL. Special Nuclear Material has been made available by the PERLA Laboratory at JRC Ispra where the tests were performed.

In Table I the SNM samples used in this work are listed. It is interesting to note that the 6g Pu samples CBNMxx are expected to emit neutrons at the rate of 800-5000 neutron/s depending on the isotopic composition, the estimate of the nominal gamma emission being more difficult due to the absorption of the metallic enclosure of the samples.

SNM	Code	Weight (g)	Mass Fraction of relevant isotope
Plutonium	CBNM61	6.6	^{239}Pu 62,5%
	CBNM70	6.7	^{239}Pu 73,3%
	CBNM84	6.7	^{239}Pu 84,4%
	CBNM93	6.6	^{239}Pu 93,4%
MOX	ENEA01	1011 UO_2 168.2 Pu	^{239}Pu 66,4%
Uranium	LU102	388	^{235}U 1,0%
	UP899S	46,4	^{235}U 89,9%
	LU25	2500	^{235}U 2,5%
	LU44	2500	^{235}U 4,4 %

Table I. SNM samples employed in this work

3. DETECTION IN PASSIVE MODE

As a first attempt, the detection of SNM samples was explored in passive mode using the SMANDRA multi-detector box. The sensitivity of the system in detecting weak gamma ray and neutron sources, as obtained in our Applied Physics Laboratory, is reported in [3]. The detection protocol for SNM was as follows:

a) For each measurement a background run was first performed in order to define the alarm threshold for neutrons in the NE213 detector, as well as for gamma ray in the high efficiency NaI(Tl) scintillator. Alarm thresholds correspond to 3 seconds measuring time;

b) All SNM samples were placed in front of the detector box, shielded by 6 mm of iron. The distances were adjusted so that the various sources would deliver a dose of 0,5 μSv/h at the surface of the detector box. This condition was defined for each sample by use of a Victoreen Model 451P ionization chamber;

c) For all samples, 5 or 10 minutes acquisitions were performed. Events were grouped offline into 3 s measurements using the time stamps. This process was done in order to verify the detection probability (PD) at a given confidence level (CL). Test were performed at PD=90%, CL=95% according to the prescriptions in ref. 9.

This protocol was defined in accordance with the prescriptions for hand-held radiometric system reported in [10].

3.1 Small Pu samples

The small 6g Pu samples (CBNMxx) produced alarms both for neutrons and for gamma rays satisfying the required DP. Typical count rates with the sample sources resulted several times higher than the laboratory background. The measured neutron yield is reported in Fig.1 in terms of counts per gram of plutonium sample in a minute measurement as a function of ^{239}Pu mass percent relative to total plutonium. The red line is the expected yield assuming a detection efficiency of about 10% for the neutron detector after energy windowing.

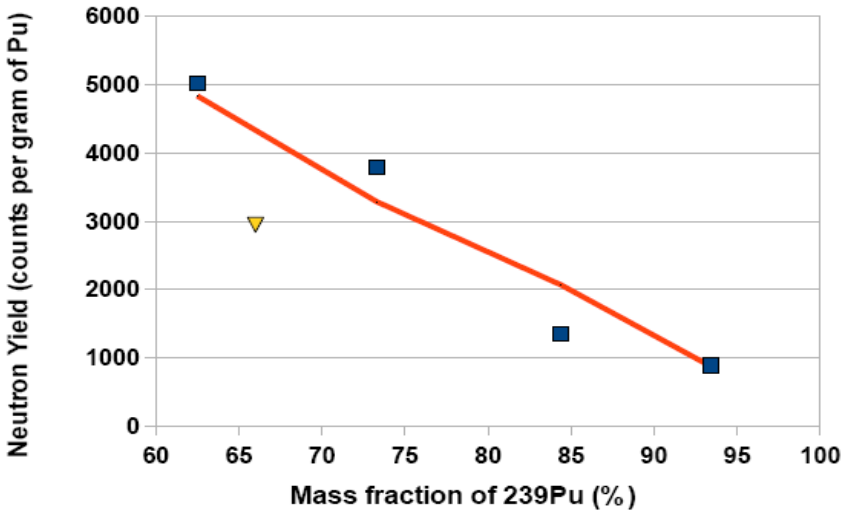

Fig.1 Measured neutron yield for 6 g calibration Pu samples (squares) as a function of the sample mass percent of the ^{239}Pu isotope relative to total plutonium. The triangle refers to a very large Pu sample (ENEA01). The line refers to yield estimate based on the sample isotopic composition. For details see the text.

Gamma rays spectra from the Pu samples have been studied making use of the superior energy resolution of the LaBr(Ce) scintillator, needed to disentangle the complex spectra [11]. Typical

results for the CBNM61 source are presented in Fig.2 where the upper panel shows the raw (energy calibrated) spectrum for a 10 minute acquisition. The high energy structure is due to the internal activation of the LaBr(Ce) scintillator (1440-1470 keV [3]).

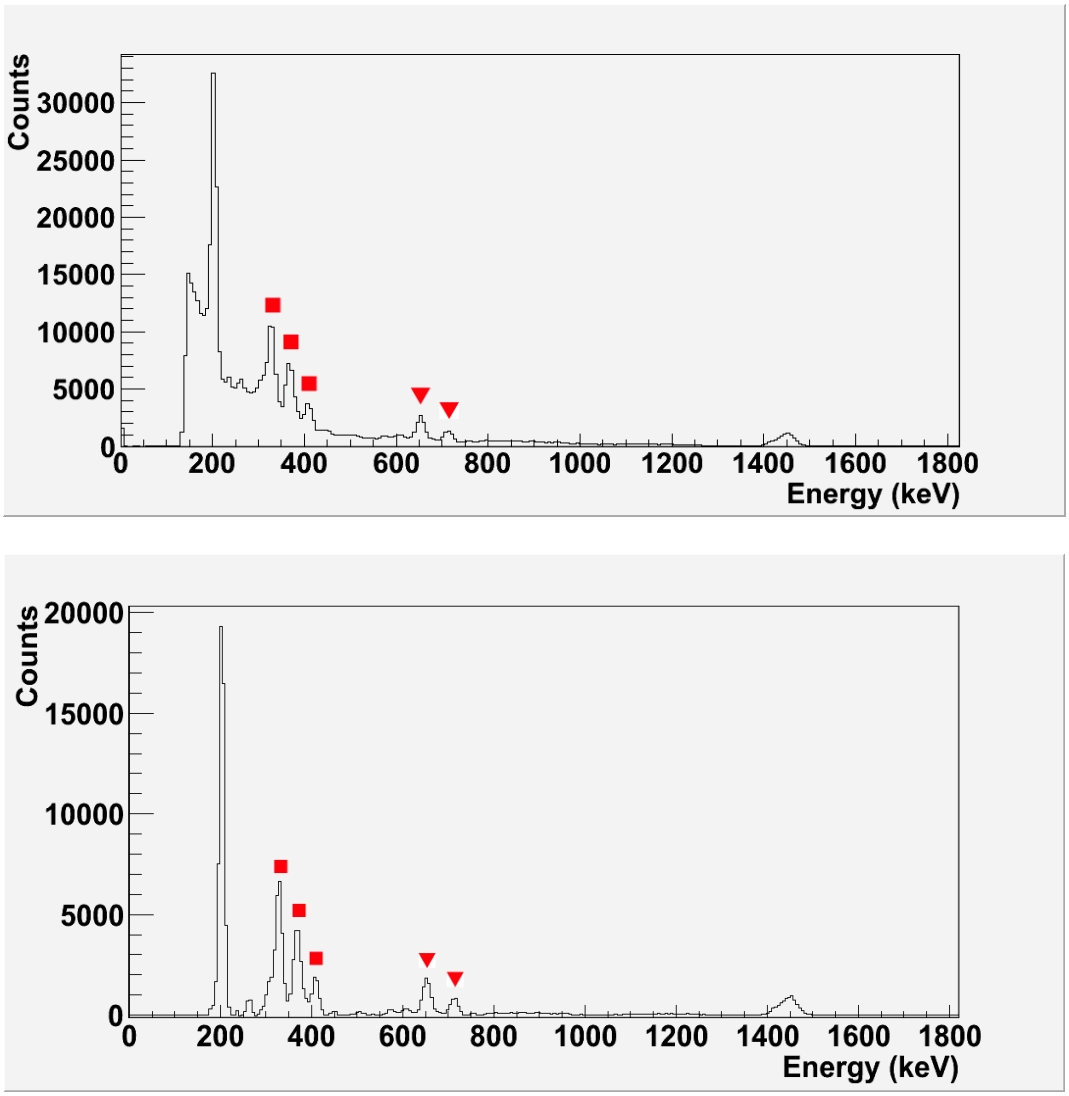

Fig.2 Gamma ray spectrum of the CBNM61 sample at different stages of the data processing. Squares and triangles mark the ^{239}Pu and ^{241}Am gamma ray transitions, respectively For details see the text.

Our software produces automatically the calibrated spectrum. Subtracting the continuous part of the energy distribution produces the spectrum in the lower panel where only peaks are left. It is also possible to subtract the ambient background as well as the internal LaBr(Ce) radioactivity. Finally, a peak search function provides the list of the gamma ray transitions with their relevant parameters (energy resolution and yield). Few gamma ray transitions are identified: the lines at Eγ=373, 414 and 451 keV which can be attributed to the ^{239}Pu decay and those at Eγ= 662 and 772 keV from the ^{241}Am decay. Moreover, the Eγ=208 keV line is due to the ^{241}Am nucleus as well as to the ^{237}U, another daughter nucleus often in secular equilibrium with ^{241}Pu. It is also interesting to note that ^{239}Pu has also a transition at Eγ=203 keV that can not be resolved with the present system [12].

The same transitions are found with the other Pu samples but the peak ratios are different according with the isotopic composition. Such features are reported in Fig. 3 in terms of yield of

the relevant ^{239}Pu lines as a function of the sample ^{239}Pu content. Fig. 4 displays the ratio between the relevant gamma lines of ^{239}Pu and ^{241}Am as a function of the ^{239}Pu content. The result is that, after the simultaneous gamma and neutron alarms, the gamma ray spectra can be used to identify the plutonium sample providing as well some rough information about the isotopic composition, especially in the very high enrichment zone.

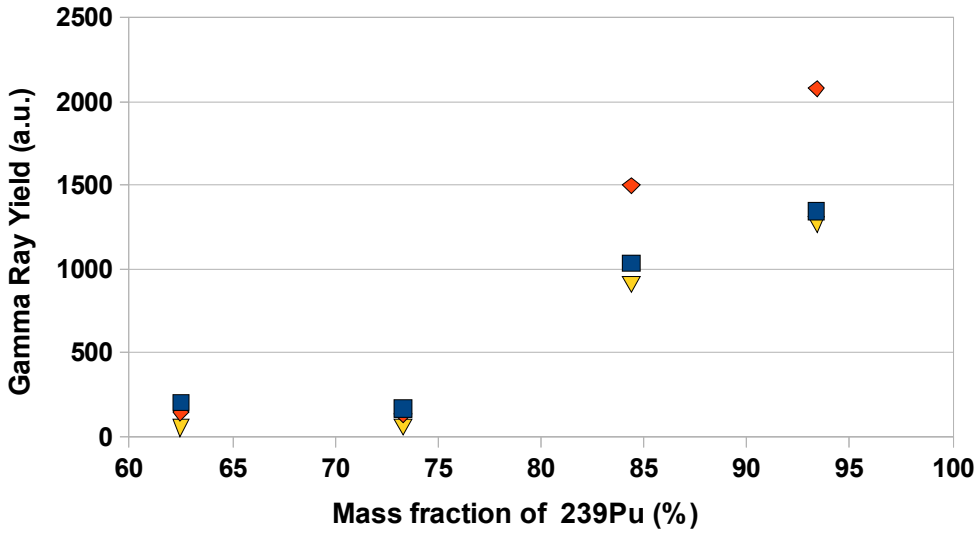

Fig.3 Yield of the relevant ^{239}Pu gamma transitions as a function of the sample mass percent of this isotope relative to total plutonium (diamond Eγ=375 keV; square Eγ=332 keV; triangle Eγ=414 keV).

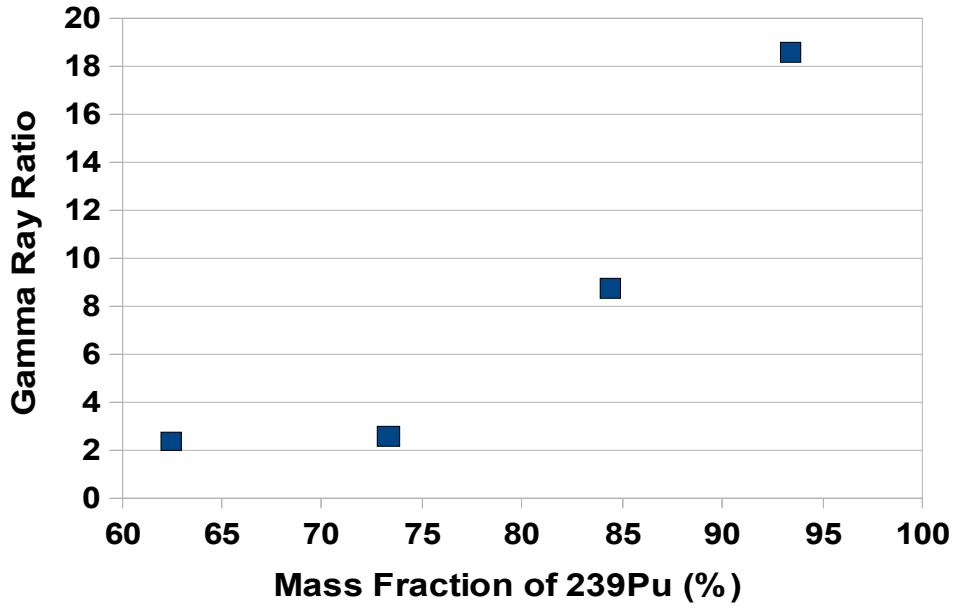

Fig.4 Ratio between the relevant ^{239}Pu (Eγ=375 keV) and ^{241}Am (Eγ=662 keV) gamma rays as a function of the sample mass percent of the ^{239}Pu isotope relative to total plutonium.

3.2 MOX sample

Signatures from a larger Pu sample have been studied using the MOX ENEA01 sample. This is particularly interesting because of the large amount of Pu present in the sample (170g) mixed with uranium oxides (1011g) and the presence of a 2.5 cm thick Pb shield around the sealed source container. The sample was positioned in accordance with prescriptions as described above. The sample releases a strong neutron signature that alarms the system providing the required DP. However, the normalized neutron yield is lower respect to the ones from 6g samples, as reported in Fig.1, due to the self absorption inside the material.

Gamma ray emission is also very strong even after the lead shield and the collected gamma ray spectrum displays clearly the expected ^{239}Pu – ^{241}Am gamma lines, as demonstrated in Fig.5.

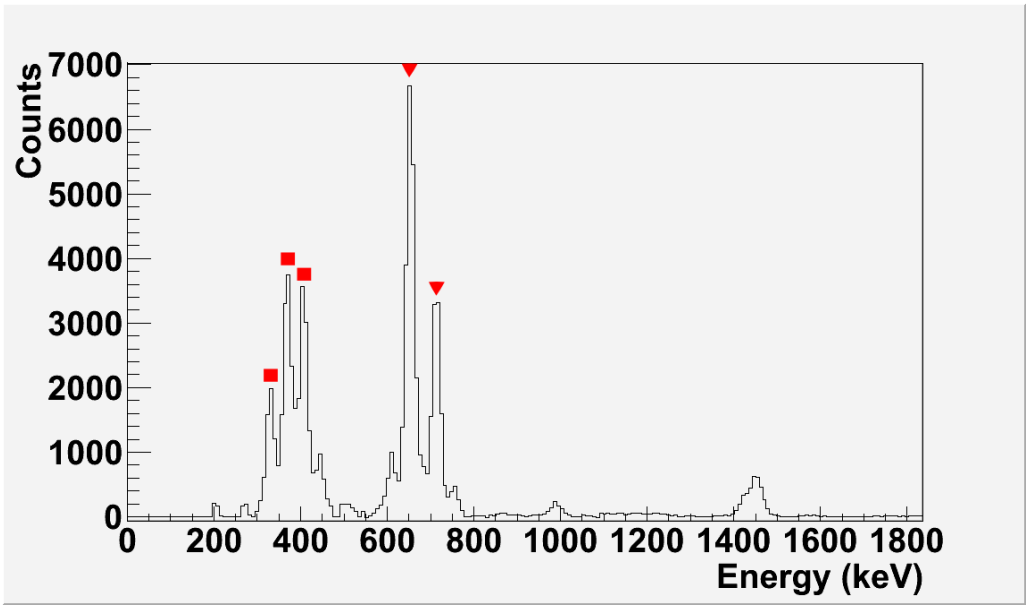

Fig. 5 Gamma ray spectrum from the ENEA01 MOX sample. Squares and triangles mark the ^{239}Pu and ^{241}Am gamma ray transitions, respectively.

3.3 Uranium samples

Uranium samples LU102 and UP899S were used to investigate the response of the system operated in passive mode to SNM with different neutron/gamma ratios. The intensity of gamma ray emission from the sample is sufficient to yield an alarm, whereas neutron emission resulted to be only about twice the laboratory background. Consequently long measuring times are required in order to get a neutron alarm with the required confidence level. As for the gamma ray signatures, measured spectra are reported in Fig. 6. In the highly enriched sample, the $E\gamma$=186 keV transition emitted in the decay of ^{235}U is clearly seen, whereas for the low enrichment sample LU102 two transitions are seen at $E\gamma$=767 and 1001 keV emitted in the decay of the ^{234m}Pa nucleus which is in secular equilibrium with the ^{238}U nucleus.

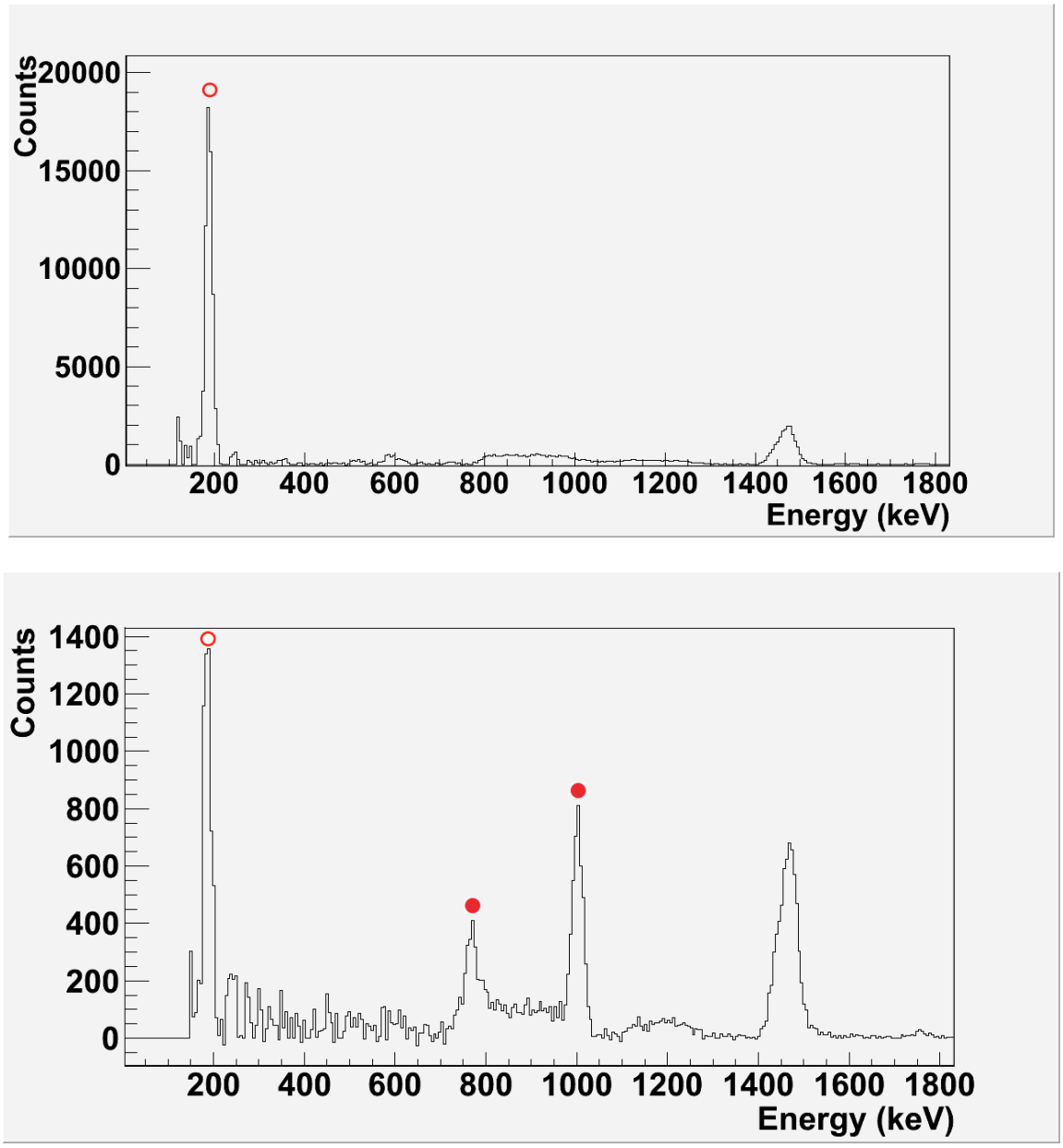

Fig.6 Gamma ray spectra from UP899S (top) and LU102 (bottom) samples. Circle and dots mark the ^{235}U and ^{238}U gamma ray transitions, respectively

3.4 Passive measurements results

As shown in this section, the Pu samples produce neutron as well as gamma ray alarms in the detection system when the dose delivered at the detector surface is 0,5 µSv/h. In the same condition the U samples produce also a clear gamma ray alarm, being the neutron emission too weak. In both cases the LaBr(Ce) gamma ray spectra provide hints on the isotopic composition of the sample. It is worth considering how this information is modified by the presence of shielding materials.

The effect of different materials on the neutron emission of a source hidden in a cargo container is discussed in detail in ref. 7 and we refer to this work for the attenuation of the neutron signal of a Pu sample. However, it is interesting here to consider in more detail the gamma ray signal from the samples studied in this work when shielded with heavy metals. This is shown in Fig. 7 where

the effect of the attenuation due to lead shielding is detailed for the characteristic gamma rays emitted from a 1g source of weapon grade plutonium (93% ^{239}Pu) and uranium (93% ^{235}Pu). In case of the WGPu, the ^{239}Pu and ^{241}Am transitions (Eγ=414 keV and Eγ=662 keV) have still a yield of about 100 Hz after 2.5 cm of shielding making the detection possible at close contact. However, the ratio between the ^{239}Pu/^{241}Am transition is modified from R=18 with no shield to R=0.8 with 2.5 cm lead providing a false hint on the isotopic composition of the sample as shown in Fig.4.

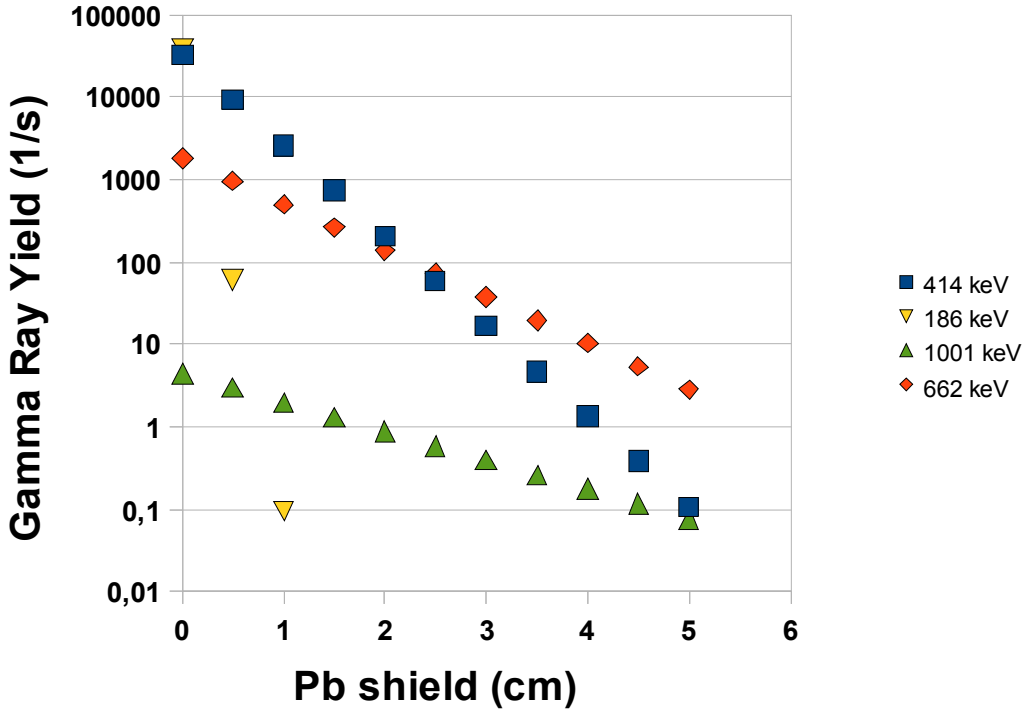

Fig.7 Gamma ray yield from 1g weapon grade plutonium and uranium samples as a function of the thickness of lead shield (diamond ^{241}Am Eγ=662 keV; square ^{239}Pu Eγ=414 keV; yellow triangle ^{235}U Eγ=186 keV; green triangle ^{238}U Eγ=1001 keV).

Moreover, the photon signature from highly enriched uranium is extremely weak even after 1 cm lead due to the low energy of the ^{235}U transition and the intrinsic low yield of the ^{238}U one. Also in this case the lead shield causes a strong change in the isotopic composition derived from the gamma ray spectrum.

Summarising, the detection of uranium samples in passive mode seems to be difficult in case the sample is shielded with high Z material that will attenuate significantly the gamma signature from the source. Being the neutron signal weak, shielding uranium with low Z materials seems to be superfluous in masking the sample. Detection of uranium with active interrogation is the subject of the next section.

4.ACTIVE INTERROGATIONS

In active interrogations the associated particle detector signal is also processed in the V1720 card. The alpha particles emitted in the ^{3}H(^{2}H,^{4}He)n reaction are indeed detected in a fast YAP(Ce) scintillator embedded in the EADS SODERN TPA17 neutron generator, coupled to an

external HAMAMATSU R1450 PMT. The complete SMANDRA system including the passive detector unit as well as the box containing the neutron generator is shown in Fig. 8.

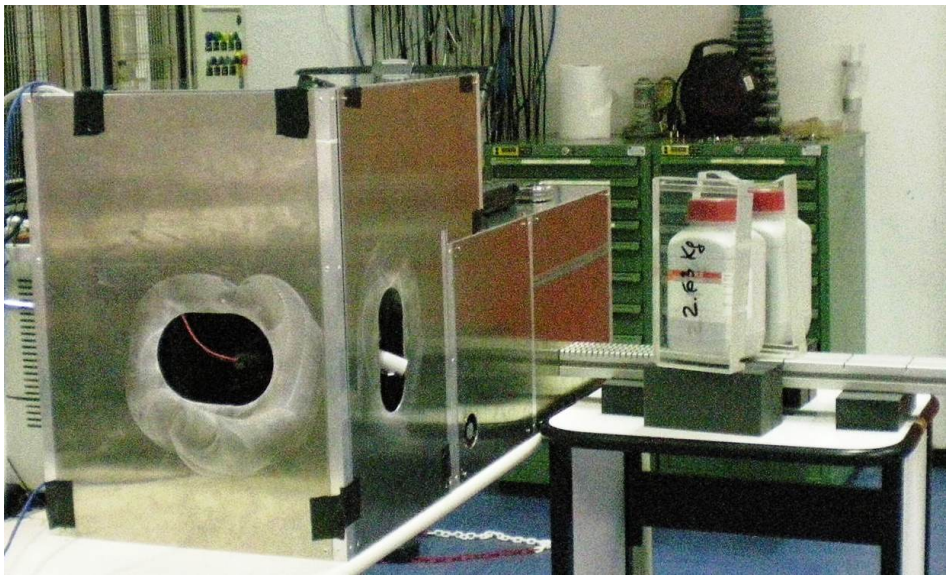

Fig.8 Active interrogation tests with SMANDRA.

The associated particle detector covers a fraction of solid angle of about 1 x 10^{-3} of 4π so that a rate of 10 kHz is expected in the operation of the neutron generator at a total intensity of 10^7 neutron/s, the limit being imposed by the laboratory license. In the above conditions, the spot of the tagged neutron beam produced by the TPA17 generator at the object position, located about 30 cm from the detector box surface, has been measured to be about 15 cm in diameter [FWHM].

In the active mode operations we stored directly all single events processed by the V1720 card running at a typical total rate of about 50 kHz, writing only the most significant part of the digitized signals. Off-line software analyzes the event files reconstructing the coincidence events and the time correlation between detectors. The time interval from the start time of the digitization and a given fraction of the front part of the signal is determined for each detector, correcting for the amplitude effects. This analysis yields a time resolution better than the V1720 sampling bin (4 ns). Laboratory tests using gamma-gamma coincidences with a ^{22}Na source and a fast plastic as trigger detector are δt=1.15 ns [FWHM] for LaBr(Ce) and δt=5.4 ns [FWHM] for NaI(Tl), respectively , with the lower threshold discrimination set at about 500 keV.

In the active interrogation tests the two large U samples LU25 and LU44 were employed together with a 16,7 kg iron cylinder, a 6,7 kg lead brick and a sample of about 10 kg organic material made of 50% Plexiglas and 50% melamine powder.

Interrogation runs lasted 10 minutes. In some cases few interrogation runs were performed for the same sample.

Typical results for U samples are reported in Fig. 9 for the LaBr(Ce) scintillator in coincidence with the associated alpha particle detector.

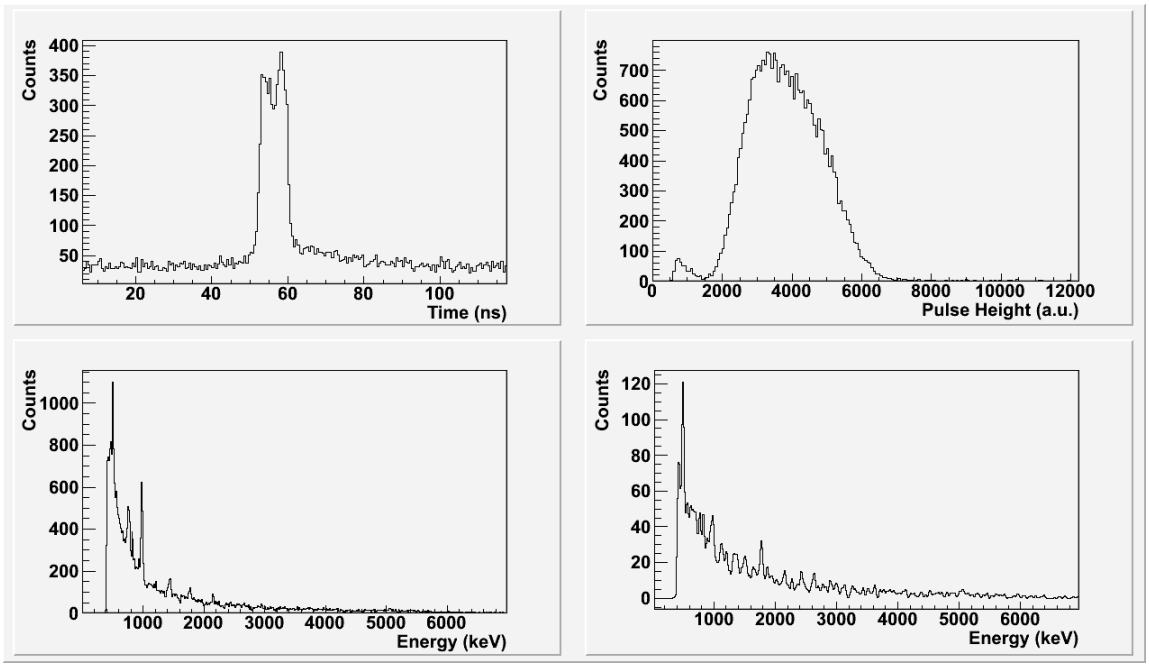

Fig. 9 LaBr(Ce) spectra measured in the active interrogation of the LU44 sample. For details see the text.

The spectrum of the alpha particle events detected by the YAP:Ce scintillator is reported in the upper right panel, whereas the inclusive gamma ray spectrum from the LaBr(Ce) detector is in the lower left panel, showing the well known pattern of emission from ^{238}U at Eγ=767 and 1001 keV. The time distribution of the coincidences (upper-left panel) exhibits a double peaked structure due to the detection in the LaBr(Ce) detector of gamma rays and neutrons from the irradiated sample. Finally the energy distribution of the gamma ray in prompt coincidence mode (lower right panel) shows no relevant structures that can be used to identify directly the uranium nuclei. The situation in irradiating iron, lead or organic material, is shown in Fig. 10. In this case, obviously, the spectrum of the LaBr(Ce) detector does not show signatures due to the internal radioactivity of the sample. Moreover, the coincident spectra of iron and organic exhibit the well known gamma ray transitions of inelastic excitation of iron (Eγ=0,847 and Eγ=1,238 MeV) and carbon nuclei (Eγ=4.44 MeV) that can be used to identify easily this type of materials [6].

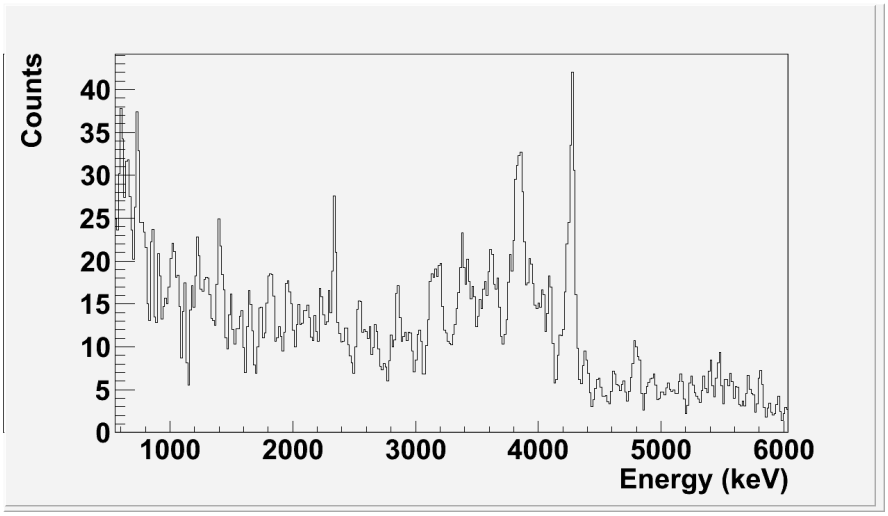

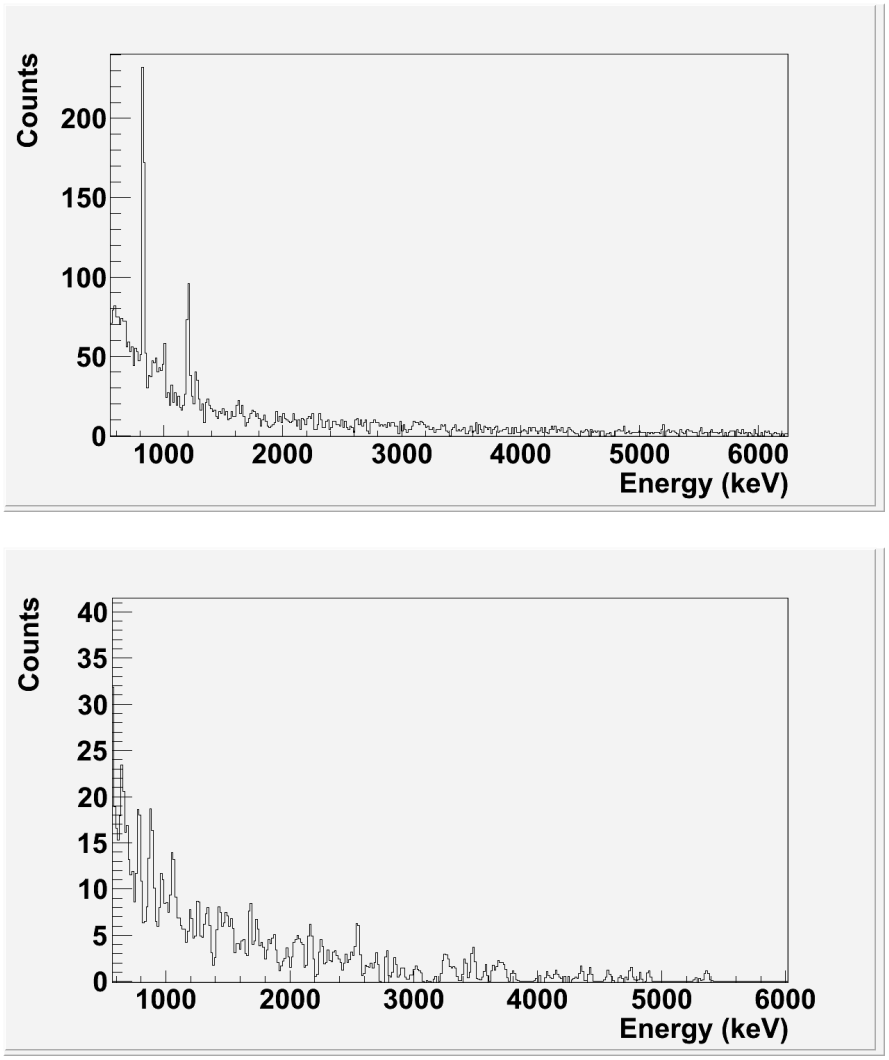

Fig.10 LaBr(Ce) gamma ray spectra in coincidence with the associated alpha particles for organic (top), iron (centre) and lead (bottom) samples.

The LaBr(Ce) coincident spectrum of the lead sample shows some structures that can be attributed to transitions in Pb isotopes as the well known Eγ=2.61 MeV in ^{208}Pb. However the coincident discrete gamma ray spectrum alone seems to be hardly usable to distinguish between Pb and U. Consequently we have explored other signatures collected by our detection system.

The time spectrum of the NE213 detector in coincidence with the associated alpha particles shows for each sample a very narrow peak due to prompt coincidences, mainly due to neutron induced gamma rays, well separated by a second larger bump due to secondary neutrons produced by the 14 MeV neutron beam, as shown in Fig.11 in case of irradiation of the LU44 sample (upper left panel). Such secondary neutrons are associated to fission (n,f) as well as (n,xn) reactions. The pulse height distribution both in single and coincident mode (lower left and right panels) does not provide useful information whereas the pulse-shape discrimination (upper right panel) is used to discriminate gamma rays and neutrons in addition to the time of flight information. We then derived the number of the detected gamma rays and neutrons from the particle discrimination algorithm after windowing the time difference between the alpha particle and the liquid scintillator signals. This allows a very good discrimination between the two types of events.

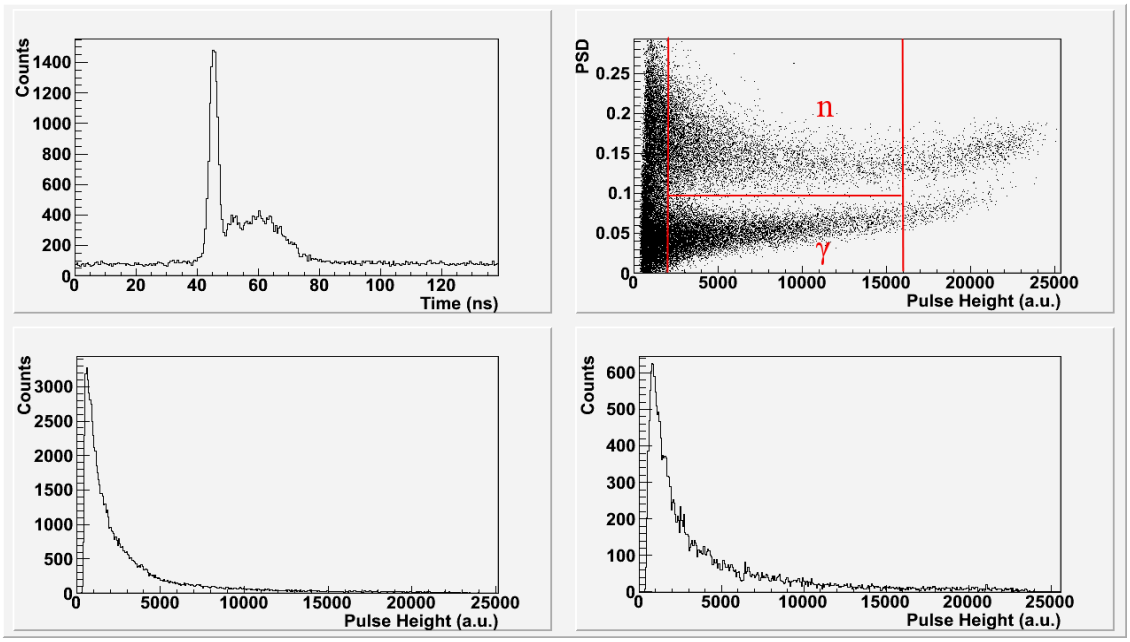

Fig.11 NE213 spectra measured in the active interrogation of the LU44 sample. For details on the panels see the text. In the upper right panel, the Pulse Shape Discrimination (PSD) parameter is reported versus the scintillator pulse height. In this case PSD is the ratio between the delayed light component and the total light, computed by using the two integration gates provided directly by the V1720 FPGA, see ref. 3 for details. Lines in the panel define the areas for accepted gamma ray and neutron events.

The yields obtained in this way, normalized to sample weight, ratio sample-beam area and measuring time are displayed in Fig.12 in terms of correlation between the number of gamma rays and neutrons detected in the liquid scintillator for each sample.

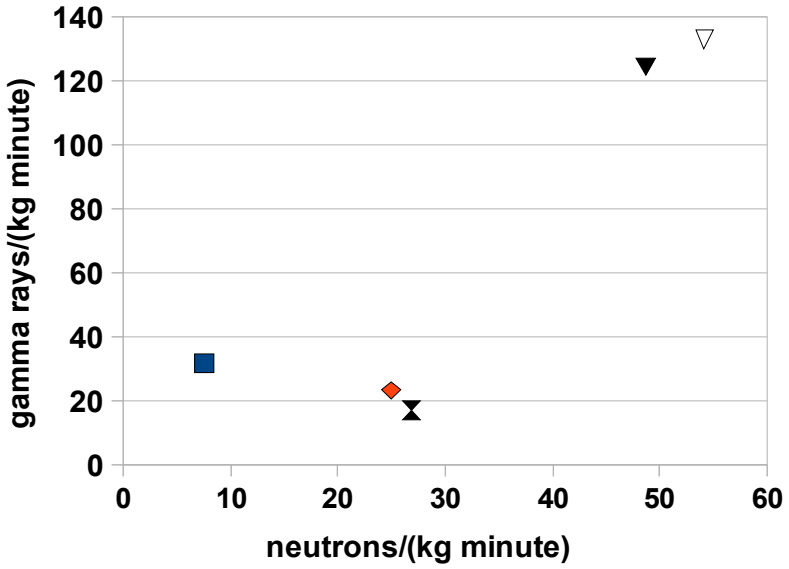

Fig.12 Correlation between the normalised neutron and gamma ray yields measured in the NE213 detector: the square refers to iron, the diamond to lead, the cross to organic and the triangles to uranium (full triangle LU44, empty triangle LU25). Data are relative to 1 kg sample for 1 minute irradiation.

It is interesting to note that the relative number of detected gamma rays and neutrons for each sample is correlated to the relevant neutron and gamma production cross sections for each elementary sample that is shown in Fig. 13. The data in Fig.13 have been obtained by using directly the relevant secondary neutron producing cross sections from the ENDF/B-VII data files [13] properly multiplied by the average number in the exit reaction channel. Gamma ray producing cross section for lead and iron are simply obtained by summing the production cross section for discrete gamma rays reported in [6] whereas uranium data are from a Los Alamos report [14]. In evaluating the gamma ray production cross section the effective threshold in the detector has been considered.

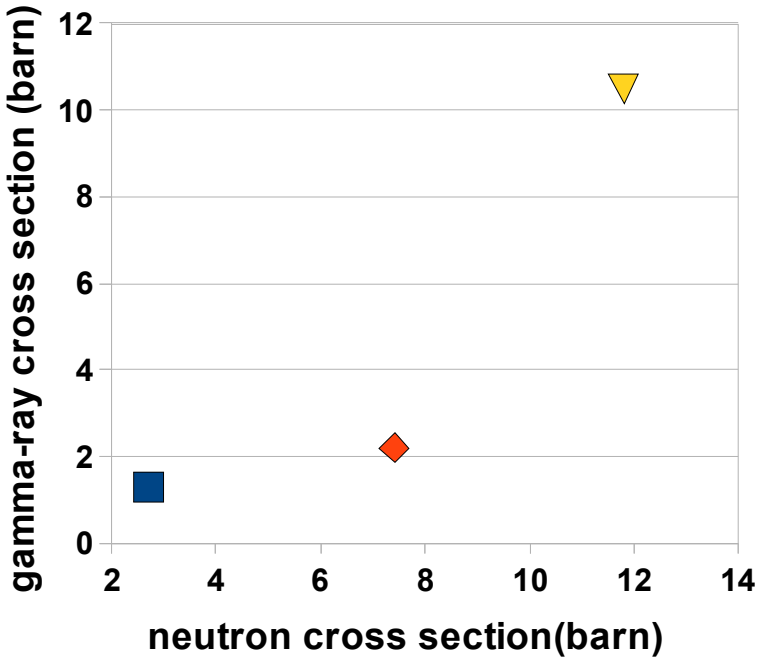

Fig. 13 Correlation between neutron and gamma-ray production cross section: the square refers to iron, the diamond to lead and the triangle to uranium. For details see the text.

The similarity between the experimental data of Fig. 12 and the cross section estimate is striking. The difference between uranium and materials commonly used for shielding is so large that some uncertainties in the cross section estimates seem to be negligible.

As a conclusion, the empirical correlation displayed in Fig.11 shows that, taking into account sample mass and area, it is possible to discriminate uranium from other materials using only the liquid scintillator data. The interrogation with tagged neutrons is able to provide evidence for an anomalous emission of gamma rays and neutrons due to the presence of uranium. This could be used also in investigating the content of a sealed lead cask able to shield the characteristic gamma ray decay of a uranium sample. In this case, a 2 cm lead shield reduces the gamma ray emission from uranium by a factor 0.2 [15], close to the lead data point in Fig. 12, whereas the neutron yield is attenuated only by about 20%, as resulted in recent laboratory tests with a ^{252}Cf sources. Consequently uranium detection would mainly relay on the excess neutron yield.

In case of the inspection of a suspect volume, as the case of cargo container, the tagged neutron technique allows to define a voxel inside the total volume. In this case it is questionable that a representation as that in Fig. 12 could be applied to search for uranium since geometry and mass of the suspect object are not a priori known. Moreover, the material in the container around the

object would attenuate the primary tagged neutron beam as well as the neutron induced reaction product, as discussed in ref. 16. This might result in a reduction of the difference between nuclear and non-nuclear materials

Consequently, new observables are required to evidence the presence of fissile material. In such case the coincident gamma ray spectrum of LaBr(Ce) easily identifies the presence of organic or iron based material through the well known gamma lines. Obviously, since the latter materials are often used to shield uranium, a method is needed to firmly identify the signal of the nuclear material inside the shield.

Similarly, in order to discriminate between lead and uranium samples, for which no discrete coincident gamma rays in the LaBr(Ce) detector are usable, a more accurate analysis is needed assuming that the radioactive decay pattern of U nuclei could be shielded thus not providing an alarm.

In order to obtain a discrimination plot, triple coincidences between the associated alpha particle, the liquid scintillator and the large volume NaI(Tl) detector were analyzed. The idea is to verify whether the multiplicity of gamma rays and neutrons emitted in the fission of ^{238}U provides a signature different from that of Pb nuclei for which neutron multiplication is due only to (n,xn) reactions.

Typical experimental data obtained in reconstructing such triple coincidence events are displayed in Fig. 14 for the uranium sample.

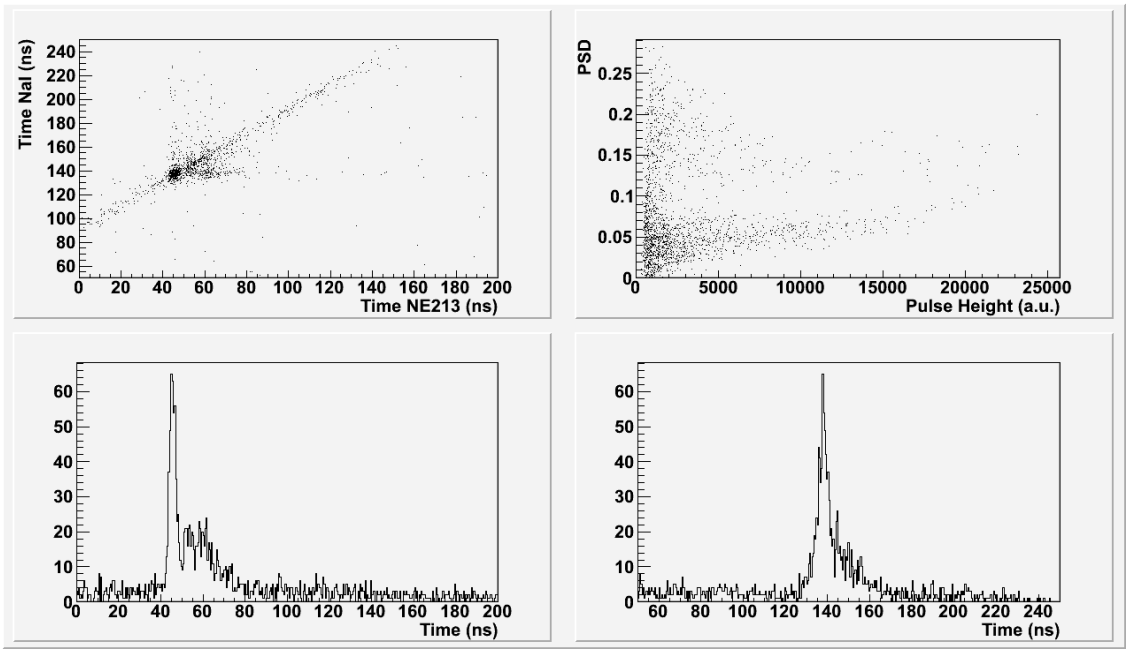

Fig.14 Triple coincidence events between the associated alpha particle, the NE213 and the NaI(Tl) detectors. For details see the text.

The lower panels report the time correlation between alpha particle and NE213 (left) and alpha particle and NaI(Tl) (right) for all events in triple coincidence. A clear peak, mainly due to gamma rays , is seen at 45 and 140 ns relative time for the NE213 and the NaI(Tl) detectors, respectively, followed by a broad distribution due to the secondary neutrons. The superior time resolution of the liquid scintillator allows us to separate more clearly the two components. In the upper right panel the NE213 neutron-gamma discrimination 2-D plot and in the upper left panel the 2-D time correlation between the coincidence time distributions are reported. The latter plot is particularly interesting since it shows clearly the structures due to different combinations between neutrons and gamma rays recorded in both detectors and the distribution of random coincidences.

Moreover, cross talk between the two detectors is also seen, due to particles scattered from one detector to the second one. Such events are generating the points on the diagonal of the 2-D plot. The relative yield of the uncorrelated events to the correlation peaks is evident also in the time spectra (bottom panels) of the two detectors. In the following analysis, results are corrected for the time uncorrelated background.

In order to obtain a parameter without need of a normalization, the number of triple coincidences (YAP:Ce-NE213-NaI(Tl)) is divided by the number of double coincidences between (YAP:Ce-NE213). This analysis is repeated twice for gamma rays or neutrons identified in the liquid scintillator. In Fig. 15 the data obtained in this way are plotted in a 2-D representation of neutron events against gamma events for the different samples explored in this work. This empirical representation results in the grouping of the sample in three regions. Lead and organic material exhibit a high probability of triple coincidence for gamma ray events (in the NE213 detector) but low for events involving neutrons. Iron is characterized by a larger probability for neutron coincidence events compared to previous samples but lower for gamma rays. Finally the two uranium samples have the largest probability for neutron triple events but an intermediate value for the gamma rays compared to all previous samples. As a result, clear distinction between uranium and other samples is obtained.

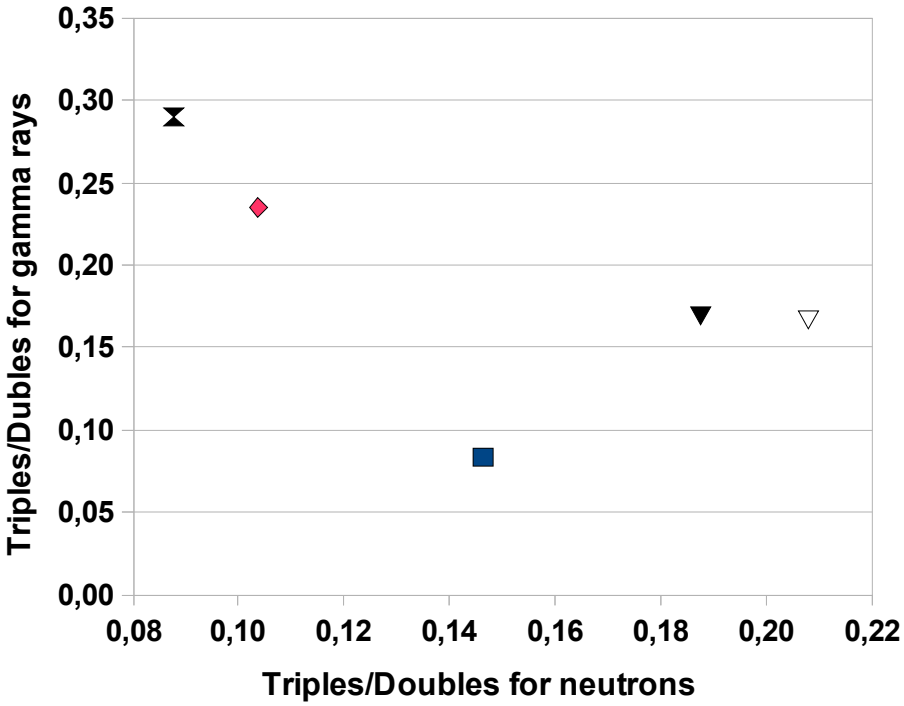

Fig.15 Correlation between the triple coincidences (alpha particle-NE213-NaI(Tl) detectors) and double coincidences (alpha particle-NE213 detectors) for neutrons and gamma rays identified in the liquid scintillator. The square refers to iron, the diamond to lead, the cross to organic and the triangles to uranium (full triangle LU44, empty triangle LU25). For details see the text.

It is worth considering that the result in Fig.15 is strongly dependent on the geometry of the present detection system and the role of the large NaI(Tl) is that of a simple counter in coincidence with the liquid scintillator. Since the efficiency of the NaI(Tl) for neutrons is supposed to be lower than that for photons, we are comparing mainly the probability that a gamma or neutron event identified in the liquid scintillator is accompanied by an additional

gamma ray in the NaI(Tl). This indicates that for uranium samples neutron events have a larger probability of being accompanied by a gamma ray. This suggests a correlation with the presence of an induced fission event.

However, the possibility of using this method in case of cargo container inspection or even in the case of a lead shielded uranium sample need to be experimentally proved. It is clear, indeed, that a 2cm lead shield, as that considered previously to mask the radioactive emission of the uranium sample, would also strongly absorb the fission gamma rays reducing the contrast between a lead and a lead + uranium object. As discussed previously, the extra neutron yield from the uranium sample with respect to lead, with the larger neutron multiplicity associated with fission events, might be a more significant signature of nuclear material. In this case, adding a second liquid scintillation detector might be a solution to improve uranium detection. Finally, the effect of the container material around the object needs to be studied in order to verify the reduction of contrast between nuclear and non-nuclear objects.

5.SUMMARY AND CONCLUSIONS

The detection of special nuclear material has been tested with the mobile SMANDRA inspection system both as a high sensitivity passive spectroscopic system and as a complete active inspection system using tagged neutrons.

The detection of plutonium samples seems to be possible with passive interrogation even in case of small samples, due to the yield of gamma ray and neutrons.

On the other hand it is well known that detection of uranium is much more difficult on one side because of the low neutron yield of this material, on the other side since the gamma ray yield of highly enriched U samples could be easily shielded. In this case active interrogation is needed.

Results reported in this paper show that the SMANDRA inspection system is able to provide signatures for the discrimination of uranium against heavy metals (as lead) by looking at the absolute gamma and neutron yield in coincidence with tagged neutrons or at correlations between detectors. This has been experimentally proved only for unshielded samples. The possibility of extending this technique to masked samples or samples hidden in large material volumes as cargo containers needs to be experimentally demonstrated.

It is worth mentioning that the SMANDRA system is a mobile multi-purpose spectrometric system not specifically designed to detect SNM. However the results reported might be implemented in future portable systems specifically designed to detect SNM in active mode, especially when masked samples are considered.

ACKNOWLEDGMENT

We thank Santino Frison, European Commission EC–JRC–ITU, Ispra, Italy, for the help during the measurements with the Special Nuclear Material at the PERLA laboratory. We have also to thank EADS SODERN for the loan of the neutron generator employed in SMANDRA.

REFERENCES

[1] see http://www.elsagdatamat.com/PDF/EDLink34.pdf

[2] S. Pesente, G. Nebbia, M. Lunardon, G. Viesti, S. Blagus, K. Nad, D. Sudac, V. Valkovic, I. Lefesvre, M.J. Lopez-Jimenez, Nucl. Instrum. and Meth. B241 (2005) 743–747.

[3] D. Cester , D. Fabris, M. Lunardon, S. Moretto, G. Nebbia, S. Pesente, L. Stevanato, G. Viesti, F. Neri, S. Petrucci, S. Selmi, C. Tintori, to be published in the IEEE Proccedings of the 2011

2nd International Conference on Advancements in Nuclear Instrumentation, Measurement Methods and their Applications, Ghent (Belgium) 6-9 June, 2011.

[4] R. Nicolini, F. Camera_, N. Blasi, S. Brambilla, R. Bassini, C. Boiano, A. Bracco, F.C.L. Crespi, O. Wieland, G. Benzoni, S. Leoni, B. Million, D. Montanari, A. Zalite, Nucl. Instrum. and Meth. A582 (2007), 554–561 and references therein.

[5] B.D. Milbrath_, B.J. Choate, J.E. Fast, W.K. Hensley, R.T. Kouzes, J.E. Schweppe, Nucl. Instrum. and Meth. A572 (2007) 774–784.

[6] W. ElKanawati, B.Perot, C.Carasco, C.Eleon, V.Valkovic, D.Sudac, J.Obhodas, G.Sannie, Applied Radiation and Isotopes 69 (2011) 732–743.

[7] R. T. Kouzes, E. R. Siciliano, J. H. Ely, P. E. Keller, R. J. McConn, Nucl. Instrum. and Meth. A 584 (2008) 383–400.

[8] R. T. Kouzes, J.H. Ely, A. Seifert, E. R. Siciliano, D. R. Weier, L. K. Windsor, M. L. Woodring, J. Borgardt, E. Buckley, E. Flumerfelt, A. Oliveri, M. Salvitti, Nucl. Instrum. and Meth. A 587 (2008) 89–100

[9] D. Gilliam et al., J. Res. Natl. Inst. Stand. Technol. **114** (2009) 195-199.

[10] M. Voytchev, P. Chiaro, R. Radev, Radiation Measurements 44 (2009) 1–5

[11] J. P. Sullivan, M. W. Rawool-Sullivan, T. R. Wenz, Journal of Radioanalytical and Nuclear Chemistry, Vol. 276, (2008) 699–705

[12] high resolution gamma ray spectra are available at the site http://www.radiochemistry.org/periodictable/gamma_spectra/

[13] M.B. Chadwick et al., Nuclear Data Sheets 107 (2006) 2931–3060

[14] L. Stewart, R. E. Hunter, Report LA-4918 UC-34, July 1972

[15] considering the average energy of fission gamma rays of about 1 MeV, see T.E. Valentine, Report ORNL/TM 1999/300, 1999.

[16] C. Carasco, B. Perot, G. Viesti, V. Valkovic, D. Sudac, S. Bernard, A. Mariani, J.-L. Szabo, G. Sannie, M. Lunardon, C. Bottosso, S. Moretto, S. Pesente, P. Peerani, V. Sequeira, M. Salvato, Nucl. Instrum. and Meth. A 582 (2007) 638–643.